Component Energy Modelling for Machine Tools

Berend Denkena , Henning Buhl , Bengt Torben Gösta Rademacher *

Posted Date: 13 March 2026

doi: 10.20944/preprints202603.1106.v1

Keywords: machine tool; energy modelling; energy efficiency; component models; load profile; mist extractor; soft starters vs. DOL

 doi:10.20944/preprints202603.1106.v1

Article

Component Energy Modelling for Machine Tools

Berend Denkena, Henning Buhl and Bengt Torben Gösta Rademacher *

Institute of Production Engineering and Machine Tools (IFW), Leibniz University Hannover, Hanover, Germany
* Correspondence: rademacher@ifw.uni-hannover.de; Tel.: +49 511 762 18003

Abstract

Rising energy costs and strict CO_2 traceability regulations create demand for monitoring energy and CO_2 emissions in manufacturing. This paper presents a framework for modelling component-wise energy models with deployable accuracy. In many factories, power meters log data at a sampling rate of 1–2 Hz, so short start-up peaks of components are underestimated. Manufacturers want to exploit this information to support operational decisions, such as peak shaving and optimising energy contract costs. To enable data-driven decisions with limited measurement infrastructure, energy models must extrapolate component behavior from sparse data. The framework is based on power measurements in accordance with ISO 14955-3, ensuring that the load characteristics required for subsequent modelling are known. The measurements are then segmented, and regressions are fitted for each segment. As a case study considering the mist extractors of two different machine tools, the proposed segmentation achieved determination coefficients (R^2) of up to 0.94 in the complex ramp-up phase. The resulting models are compact, interpretable, and suited for energy monitoring on edge devices. The contribution is a reproducible framework for delivering peak-aware, component-level energy models from low-frequency industrial power meter data.

Keywords: machine tool; energy modelling; energy efficiency; component models; load profile; mist extractor; soft starters vs. DOL

1. Introduction

Improving energy efficiency is a global priority in manufacturing, driven by both rising energy costs and climate objectives [1]. Within manufacturing, metal-cutting machine tools are among the most energy-demanding assets [2]. However, a large share of this total energy demand is not directly attributable to value-adding material removal at the machine level [3]. Instead, auxiliary units such as machine cooling frequently dominate overall consumption even during cutting [4].

Despite this high energy consumption, detailed monitoring of individual components is often economically infeasible. Shop floor monitoring is usually restricted to just a few metering points. Modern machine tools typically come equipped with just one power meter at the main supply, to enable energy monitoring displayed on the human-machine interface (HMI). Typical power meters such as the Phoenix Contact EMpro (type EEM-MA370) or the Siemens SENTRON (type PAC2200) measure total effective power and phase currents, but only at low sampling rates of 1–2 Hz, which is insufficient for precise observation or demand-oriented control [5,6]. This lack of temporal resolution also often masks short power peaks, preventing manufacturers from implementing peak-shaving strategies to reduce energy contract costs. Component-level energy models are therefore required to quantify the demand and associated costs of individual units despite such limited measurement infrastructure.

This paper provides a framework applicable to modelling the energy demand of most machine tool components. The first section reviews the current state of research and categorises machine tool components by their load behaviour. Section 2 then details the materials and methods used to

 doi:10.20944/preprints202603.1106.v1

consistently measure component-level power demand. In Section 3, a case study for energy modelling is carried out on two mist extractors from different machine tools. The results include a Nyquist-aware method for peak correction for low-sampling rate data and the segment-wise synthesis of component load profiles using regression models.

1.1. Related Work

In order to improve the resolution of monitoring and to capture peaks, dedicated energy models have been developed. For metal-cutting machine tools, these models typically decompose the total demand into constant and variable consumers [7–10]. Within this framework, feed drives and cooling units are identified as major contributors to energy consumption. However, while drives are modelled in detail, auxiliary units are often simplified to constants or overhead factors, despite their large share of the overall energy demand [11]. A systematic approach to modelling auxiliary units individually is therefore missing.

Auxiliary units are increasingly operated with demand-oriented control, often through the use of variable frequency drives (VFD). For example, adapting the volume flow of cooling lubricants via a VFD-controlled high-pressure pump has shown energy savings of up to 89% for this component [12]. However, such control is not available for all components. It often represents an expensive optional feature, or is only offered for newly released units that are not yet present in the installed machine fleets. In operation, many auxiliary units exhibit an approximately constant power demand. Therefore, it is not economically feasible to equip all of them with measuring devices.

Within the subgroup of auxiliary units, mist extractors, for example, represent an often underestimated share of around 5–10% of the total electrical energy demand during the machine tool operating state PROCESSING [13,14]. Models for this component are usually reduced to a simple constant. A detailed, experimentally grounded characterization of mist extractor load profiles, particularly their start-up behaviour, is thus still missing. This start-up phase is especially relevant because global load peaks occur during it, driving power contract costs. If constants are assumed in the model, detailed information on peak magnitude and timing is lost.

In order to enable consistent assessment of machine tool energy demand, the ISO 14955 series was introduced [15,16]. ISO 14955-1 and ISO 14955-3 provide a framework that defines system boundaries. These boundaries specify which components and energy flows (e.g., compressed air, cooling lubricant) are in scope. They also establish a basis for assigning consumption to operating states of machine tools (e.g., OFF, READY, PROCESSING). However, these standards do not describe how to derive compact component models from measurements, especially when only low-frequency data at the main supply is available.

Regarding data processing, the non-intrusive load monitoring (NILM) community has developed methods to disaggregate building-level meter data into appliance-level loads [17–19]. Originating in building management, these approaches show strong potential for transfer to machine tool energy monitoring, enabling disaggregation of total consumption to individual component loads. They also handle the low-frequency data provided by standard power meters. In parallel, machine tool builders are experimenting with initial testing cycles to measure the load behaviour of individual components on the factory side [20]. In this context, an energy model is understood as a deployable representation of a component's load profile that can also be used to estimate peak power demand and to evaluate potential savings from alternative control strategies.

Prior work has established the importance of auxiliary units and offers concepts for modelling and standardisation. A reproducible workflow that combines the following qualities, however, has not been provided:

1. Starts from industrial 1–2 Hz data;
2. Compensates for under-sampling;
3. Segments load profiles into meaningful phases;
4. Yields compact regression models suitable for monitoring.

 doi:10.20944/preprints202603.1106.v1

Providing such a workflow, using two mist extractors with different drive technologies as a case study, is the contribution of this paper.

1.2. Classification of Machine Tool Component Energy Behaviour

In order to derive energy models that can be deployed for monitoring, reporting and peak-load management, each component is assigned to a class, which then guides the subsequent modelling approach. In general, machine tool components can be classified into four characteristic energy-consumption classes: stationary, cyclostationary, transient with plateau and non-stationary. Stationary consumers draw approximately constant power, cyclostationary consumers follow a characteristic periodic pattern and non-stationary consumers vary with motion commands and load, leading to larger fluctuations. Figure 1 illustrates these basic behaviours, following [1]:

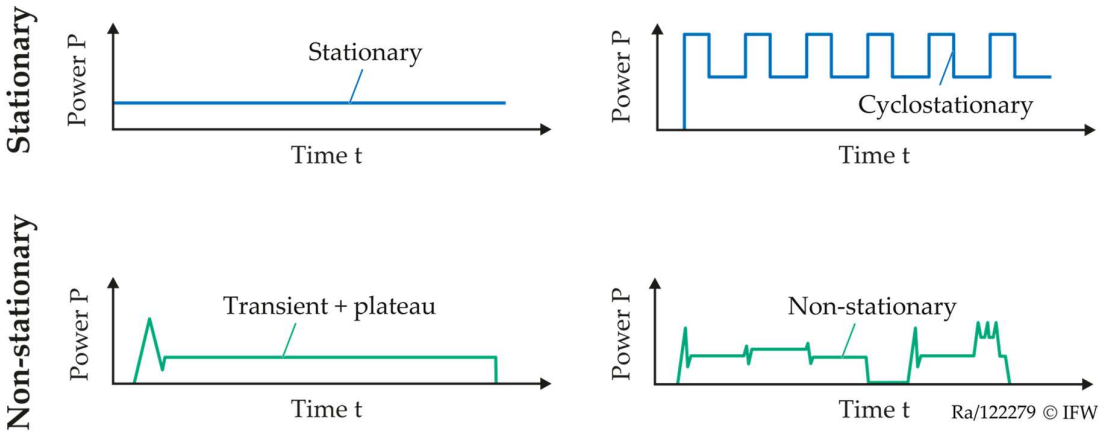

Figure 1. Classification of load profiles of machine tool components based on [1].

Based on Figure 1, all measured components can be classified to show either stationary or non-stationary energetic behaviour in the PROCESSING operating state. Table 1 summarises the findings from individual measurements and the relevant literature. Because different technological implementations of a component (e.g., control strategy or drive type) can alter its behaviour, a single component may belong to several classes:

Table 1. Classification of energetic behaviour by component considering different technologies derived from Figure 1 and the literature [21,22].

Component	Class	Technology
(Machine) cooling	Cyclostationary	Hot-gas bypass
	Non-stationary	Inverter/VFD[1] compressor
Drives	Non-stationary	Servo drives
Coolant pump	Transient + plateau	Fixed-speed pump
	Non-stationary	VFD with pressure control
	Non-stationary	VFD with flow-rate control
Oil mist extractor	Transient + plateau	Fixed-speed fans, soft starter
	Non-stationary	VFD with flow control
24V-supply	Stationary	-
Lifting pump	Transient + plateau	Infrequent runs on demand
	Cyclostationary	Float switch with hysteresis
Chip conveyor	Cyclostationary	Timed duty cycle
	Non-stationary	Load sensing cycle, VFD

[1] VFD – Variable frequency drive.

 doi:10.20944/preprints202603.1106.v1

In general, newer and typically more expensive technologies (e.g., variable-speed drives, soft starters, intelligent controls) introduce non-stationary behaviours that can reduce operating costs but require higher upfront investment. Different technologies exhibit unique power behaviours, which are only partially captured in low-frequency measurements at the main supply.

Accordingly, energy modelling approaches must be robust to handle low sampling rates. Physical component models offer process insights, while empirically built mathematical models aim to closely fit or predict the measured time series of the power profiles. The latter are often used in factory-side testing cycles where machine tool builders calibrate component models by switching components on and off while monitoring the power demand at the main supply. The framework presented in this work is directly applicable to such scenarios.

2. Materials and Methods

This section describes the instrumentation and the data-processing workflow used to develop mathematical, component-level energy models from low-sampling-rate data. To gain insight into the behaviour of the components under consideration, energy measurements are first carried out. The instrumentation and the ISO 14955-compliant measurement regime are described in Section 2.1. Second, the methods that are subsequently applied in Section 3 are outlined.

2.1. Measuring Regime and Instrumentation

The measurements in this work covered the operating states defined in the ISO 14955 framework. They complied with the prescribed system boundaries, validation runs and minimum experiment durations. For the PROCESSING operating state, the JIS TS B 0024-1 test workpiece was selected, which features face milling, slot milling and drilling operations [23]. The workpiece was machined on a DMG MORI Milltap 700 with parameter variations (a_p = 1–3 mm; f = 100–2,000 mm/min). The tooling included end mills with d = 10 mm and d = 16 mm as well as HSS drills with d = 10 mm and d = 16 mm and a 50 mm face-milling cutter with inserts. The elements of the experimental setup are shown in Figure 2.

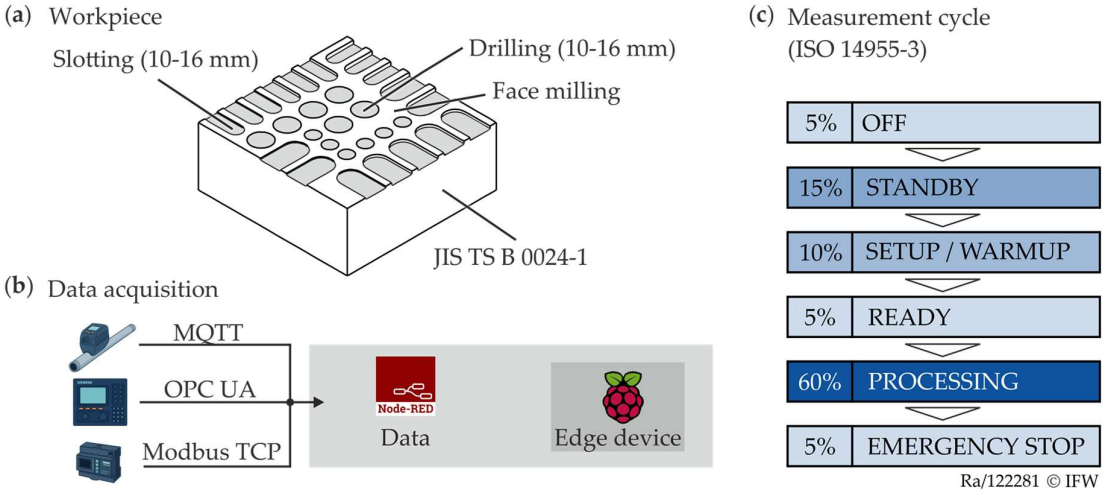

Figure 2. Elements of the measurement experiment: (**a**) JIS-workpiece, (**b**) data acquisition and the (**c**) measurement cycle according to the ISO 14955 series [15,16].

Electrical power at the machine tool's main supply and at eight electrical components was measured with Siemens SENTRON power meters of the type PAC2200 via the Modbus TCP protocol. The components measured include cooling (control cabinet chiller and central hot-gas bypass cooling unit), 24 V supply, mist extractor, high-pressure coolant pump, lifting pump, chip conveyor and the drives. In parallel, control signals (e.g., OPC UA and S7 boolean signals) were logged to time-stamp

 doi:10.20944/preprints202603.1106.v1

the activation of components such as the chip conveyor and the mist extractor. These binary traces serve as anchors for segmentation and model fitting.

As defined in ISO 14955-3, all media flows must be considered when measuring energy consumption of machine tools. Compressed air (CA) flow was therefore measured as well, using ifm SD6500 volume-flow sensors. The electrical and equivalent CA power demand during SETUP and PROCESSING is shown in Figure 3.

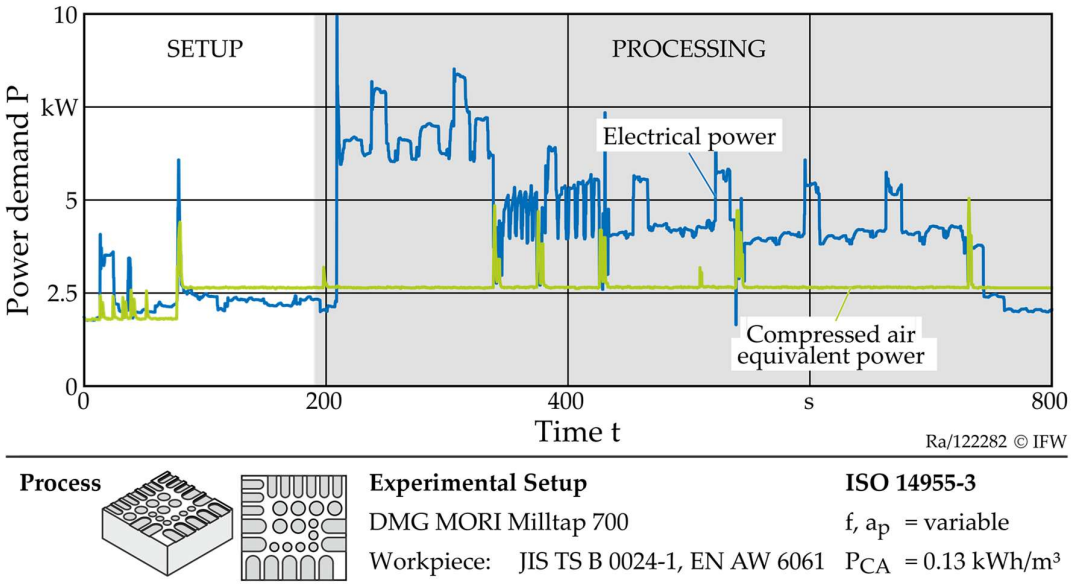

Figure 3. Comparison of electrical power demand and compressed-air-equivalent power demand [24] during SETUP and PROCESSING.

A comparison of power demands in Figure 3 reveals that electrical components exhibit higher volatility than the compressed air (CA) system. The CA power demand remains largely predictable due to the baseline of stationary sealing air and only shows short spikes caused by blowing air during tool changes. By contrast, electrical power demand fluctuates dynamically, even during SETUP before actual material removal starts. Consequently, the primary challenge in the scope of this work lies in modelling electrical components of machine tools.

2.2. Modelling Electrical Components from Industrial Power Meter Data

The remaining components consume electrical power and are measured with typical power meters operating at 1–2 Hz so that it is insufficient for precise monitoring. Figure 4 illustrates how this work derives models for electrical components from low-rate data obtained in monitoring-oriented environments. First, power peaks in the load profiles are identified and locally reconstructed using a Nyquist-aware procedure. Around each discrete maximum, a three-point interpolation is performed and then adjusted by a curvature-based bias term that compensates for under-sampling according to the Shannon-Nyquist sampling theorem. This step is marked in Figure 4 as peak correction [25–27].

 doi:10.20944/preprints202603.1106.v1

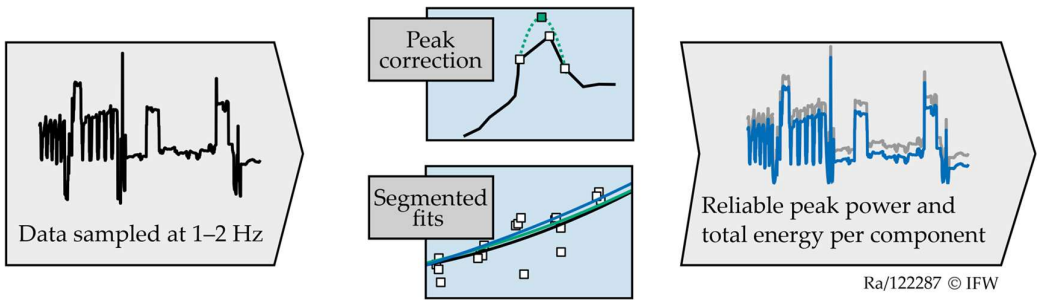

Figure 4. From low-frequency measurements to usable models: Nyquist-aware peak correction and segmented fits for more accurate peak power and energy estimation.

Second, the full profile of the component is decomposed into physically meaningful segments (e.g., starting or ramp-up). For each segment, parametric regressions are fitted, and the switching points between segments are tuned via grid search to minimise the energy deviation ΔE between the modelled and the actual energy demand E over the entire run of the component.

3. Case study: Energy Modelling for Mist Extractors

This section reports the case study on modelling the energy demand of auxiliary units, with a focus on the mist extractor. First, following the ISO 14955-3, the PROCESSING state on a DMG MORI Milltap 700 was measured to analyse the component-level power demand, as shown in Figure 5.

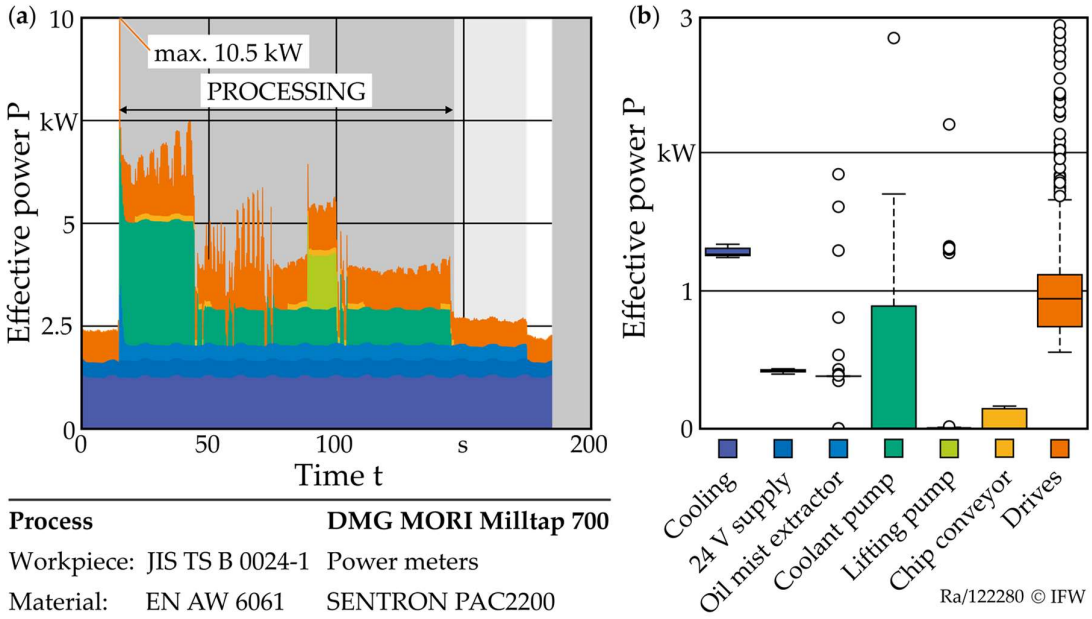

Process		DMG MORI Milltap 700
Workpiece:	JIS TS B 0024-1	Power meters
Material:	EN AW 6061	SENTRON PAC2200

Figure 5. Effective power demand of different components during PROCESSING on a Milltap 700: (**a**) stacked power profile and (**b**) component-wise box plot analysis.

In Figure 5a the power profile of the main components during PROCESSING is shown, which reveals the variable power consumption of non-stationary components such as the axis and spindle drives. Box plots show wider interquartile ranges of power demand for these non-stationary components (Figure 5b). Components like the 24V-supply and the cooling system have a much tighter spread in measured values and can thus be considered stationary or cyclostationary energy consumers.

 doi:10.20944/preprints202603.1106.v1

A potential opportunity for energy savings is indicated by the narrow interquartile ranges of the mist extractor, the chip conveyor and the lifting pump. These units draw nearly constant power when switched on. Mist extractors are used on machine tools that generate aerosols during the use of cooling lubricants in order to remove these mists. They are particularly relevant, as they are typically enabled in the entire PROCESSING operating state (i.e., while an NC program is running). Therefore, any reduction of their duty time directly leads to energy savings. The demand also varies very little during most of the PROCESSING, except for a dynamic start-up period visible in Figure 5a. A trailing sequence of 30 s, which is configurable on the HMI, is added to ensure that remaining aerosols are removed from the workspace of the machine tool before the door is opened. Mist extractors represent a case of a "transient + plateau" auxiliary unit (see Figure 1). However, their operational behaviour is not identical across different machine tools.

In the remainder of this section, the mist extractors of two different machine tools (DMG MORI Milltap 700 and DMP 70) designed for similar 5-axis milling tasks are therefore considered. Baseline lookup tables with constant power are first outlined in Section 3.1. Second, a reliable estimate of the magnitude of the peak power demand and its timestamp is derived (Section 3.2). Third, to reproduce the load profile beyond a constant-power surrogate, the load profile is segmented and segment-wise regression models are fitted. The regression is then tuned via grid search (Section 3.3), to increase the accuracy and minimize the total energy error $\Delta E = E_{model} - E_{actual}$ over the entire activity of the auxiliary unit. Section 3.4 extends the analysis to a second unit on a different machine tool, which exhibits a different start-up behaviour.

3.1. State of the Art: Lookup-Table Baseline Models

When detailed models are not available, simple lookup tables for operating state-based power demand can still provide useful data. Table 2 presents a rule-based lookup that covers the energy consumption of auxiliary units in domains where heuristics dominate. These heuristics are typically constant or linear relationships triggered by discrete signals (e.g., S7 boolean signals) or by monitored values crossing predefined thresholds.

Table 2. Extended rule-based lookup table for the power demand of auxiliary units of the DMG MORI Milltap 700.

Component	States	Trigger	Heuristic Model
Chip conveyor	Off	-	P_{Off} = 0 W
	On – (Forward)	S7 variable	P_{For} = 150 W
	On – (Reversed)	S7 variable	P_{Rev} = 150 W
Lifting pump	Off	-	P_{Off} = 0 W
	On	S7 variable	P_{On} = 1,300 W
Control cabinet chiller	Off	-	P_{Off} = 0 W
	Fan	T_C < 35 °C	P_{Fan} = 62 W
	Hot	T_C ≥ 35 °C	P_{Hot} = 570 W
24V-supply	Off	-	P_{Off} = 0 W
	Low	Operating state * ≠ SETUP	P_{Low} = 380 W
	High	Operating state * = SETUP	P_{High} = 400 W

* ISO 14955-3 defines SETUP as an activity-based state that applies while tasks such as homing cycles are being performed.

Unlike most auxiliary units triggered by the machine tool's control, the control cabinet chiller operates autonomously. The unit combines a continuously running fan drawing P_{Fan} and a compressor. A two-point controller with hysteresis monitors cabinet temperature T_C and toggles the compressor. This produces on-off cycling and between runs, the fan maintains air circulation. Because the cabinet's thermal load varies with machine activity and external heat gains, cycle timing is irregular. Also, in most machine tools, no control variable can be used to trigger a heuristic model for the control cabinet chiller. Using the level of P_{Fan} and P_{Hot} respectively, the activity of the control

 doi:10.20944/preprints202603.1106.v1

cabinet chiller can be disaggregated from the main supply as a promising subject for further work. In the following sections, the focus is on control-triggered auxiliary units, represented by mist extractors as a case study.

3.2. Power Peak Corrections

Simple lookup tables fail to resolve the transient phase of the power profile and therefore entirely miss characteristic start-up peaks, which are critical for optimising energy contracts. In this section, the power peak for the mist extractor of the Milltap 700 is therefore estimated with a three-point parabolic interpolation around the point triplet (t_-, P_-), (t_0, P_0) and (t_+, P_+) where t_i is sampling time and P_i the measured power at the time-stamp t_i. A quadratic $y = at^2 + bt + c$ is fitted to these three points, resulting in the sample peak estimate ($\hat{t}$, $\hat{P}$) as specified in Equations 1 and 2:

$$\hat{t} = -\frac{b}{2a} \quad , \qquad \hat{P} = y(\hat{t}) \tag{1), (2}$$

The resulting mathematical estimation does not account for under-sampling per the Shannon-Nyquist sampling theorem [25]. Therefore, a small bias correction, derived from a second-order Taylor expansion of the local signal around the discrete peak, is applied. Using the local curvature $\kappa = -2a$ and the local step of the parabola, defined as $\Delta_t = \min(\Delta_+, \Delta_-)$, this yields the correction term $\kappa\Delta_t^2/24$. A similar 1/24 factor appears in basic quadrature error expressions (e.g., midpoint/trapezoidal) [27]. The Nyquist-corrected peak $\widehat{P_{nyq}}$ is then obtained as specified in Equation 3:

$$\widehat{P_{nyq}} = \hat{P} + \frac{\kappa * \Delta_t^2}{24} \tag{3}$$

Peaks usually occur at the very beginning of the start-up of the mist extractor – often within the first five samples. Because logging starts when the S7 signal switches to "True", values preceding the peak sometimes lie outside the recorded window. In these cases, the point triplet is incomplete, or additional overshoot is introduced when fitting the parabola using an imputed $P_- = 0$ kW. In order to prevent this, the initial dataset of n = 10 load profiles was filtered by removing instances relying on baseline neighbours (e.g., $P_- \approx 0$ kW). This ensures that only near-peak neighbours at both t_- and t_+ are retained.

Another source of curvature outliers is asymmetric local sampling, so when the local steps on both sides of $\hat{t}$ differ ($\Delta_+ \neq \Delta_-$). To address both edge cases, the dataset is filtered using the following two quality gates, first enforcing near-peak neighbouring values (Equation 4):

$$\frac{\min(P_-, P_+)}{P_0} \geq 0.6 \tag{4}$$

Next, at least moderate time-gap-symmetry at t_0 is enforced (Equation 5):

$$\frac{\max(t_+ - t_0, t_0 - t_-)}{\min(t_+ - t_0, t_0 - t_-)} \leq 3 \tag{5}$$

The threshold values for the gates used in Equations 4 and 5 can be adjusted as required. These conditions stabilize the estimates and reduce curvature outliers, which is common for quadratic peak/time-delay interpolation in signal processing [26].

From the initial n = 10 runs, the gates retain four runs spanning air-cutting and machining of EN AW 6061. With n = 4, the median is used as an aggregator for both $\hat{t}$ and $\widehat{P_{nyq}}$, although the mean is generally preferable for significantly larger sample sizes. The findings for the corrected power peaks are summarised in Table 3:

 doi:10.20944/preprints202603.1106.v1

Table 3. Start-up peaks (median values) with sub-sample interpolation, Nyquist-corrected for the DMG MORI Milltap 700.

Condition	n	Peak time $\tilde{x}(\hat{t})$ [s]	Peak power $\tilde{x}(\widehat{P_{nyq}})$ [W]
Overall	4	Measured	Measured
		0.62 (0.18)	1,888.45 (303.42)
		CI[1] [0.35; 0.93]	CI[1] [1,362.98; 2,328.60]
		Corrected	Corrected
		0.56 (0.09)	1,975.95 (340.06)
		CI[1] [0.45; 0.74]	CI[1] [1,396.52; 2,478.73]

[1] CI – 95% Confidence interval, using the t-distribution.

With the remaining n = 4 runs, the point estimates are reported together with 95% intervals. The standard deviation across these runs is small for $\hat{t}$ (SD ≈ 0.09 s), indicating limited variability in the timing of the peak and also a more accurate prediction through the correction. Also, the median across the corrected $\widehat{P_{nyq}}$ is almost 100 W higher than the uncorrected median, which is non-negligible for peak-shaving applications.

The estimations still substantially improve upon the initial power profiles provided by the power meters at low sampling rates of 1–2 Hz. This is valuable for MES and related systems that optimize peak-load shifting by relying on accurate peak estimation. For the mist extractor, the corrected peak power is $\widehat{P_{nyq}}$ ≈ 1.98 kW occurring at $\hat{t}$ ≈ 0.56 s after activation.

3.3. Synthesis of a Full Load Profile

After estimating the magnitude of the peak power demand, in a second step the load profile is modelled to better reproduce the actual energy E. In order to achieve this, the four load profiles are synchronised to the peak, which is set to t = 0 s. This is in accordance with the two-step quality gates introduced in Section 3.2. The load profile for the Milltap 700 mist extractor can be divided into a decay (a) and a constant (b) part, as shown below in Figure 6:

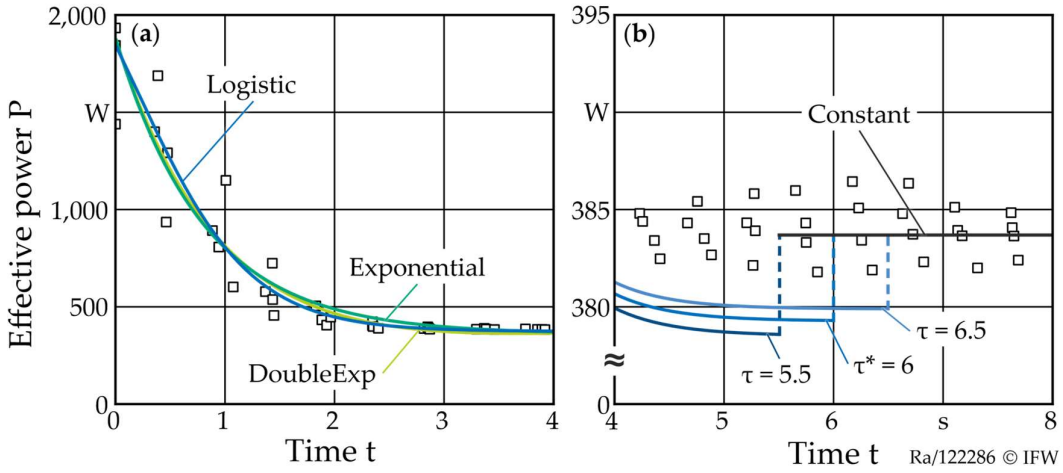

Figure 6. Model selection and cutoff time for decay: (**a**) logistic vs. exponential fits and (**b**) optimization of τ for the logistic fit via grid search.

The optimal regression parameters are highly dependent on the switch point between segments, when the decay (a) ends and the constant segment (b) begins. To determine the switching timestamp τ and to improve transferability to other power profiles that may not be cleanly separable, a grid search over candidate τ values was employed. The asymptotic constant P∞ is set to the mean of the last 10 samples. As shown in Figure 6 (b), the best fit (logistic) slightly undershoots the measured

 doi:10.20944/preprints202603.1106.v1

points at the optimal value of $\tau^* = 6$ s. Changing τ however also influences the fit closer to the load peak. The full resulting regression parameters of the grid search are provided in Appendix A1.

3.4. Transfer to a Different Machine Tool (DMP 70)

In practice, there are different starting behaviours beyond the direct-on-line starter (DOL) encountered with the Milltap 700, which immediately peaks right after activation of the component. By contrast, the mist extractor of a different 5-axis CNC milling centre, the DMP 70, shows a characteristic soft-start response. The more gradual increase in power demand reduces start-up stresses and helps protect electrical and mechanical subcomponents. It also supports peak-shaving applications by limiting the peak power $\hat{P}$. Table 4 reports how these differences manifest in the corrected start-up peaks, obtained using the method from Section 3.2:

Table 4. Start-up peaks (median values) with sub-sample interpolation, Nyquist-corrected for the DMG MORI DMP 70.

Condition	n	Peak time $\tilde{x}(\hat{t})$ [s]	Peak power $\tilde{x}(\widehat{P_{nyq}})$ [W]
Overall	4	Measured	Measured
		16.05 (1.15)	626.18 (6.60)
		CI[1] [14.56; 18.20]	CI[1] [613.99; 634.99]
		Corrected	Corrected
		15.94 (1.16)	634.98 (4.75)
		CI[1] [14.42; 18.11]	CI[1] [626.58; 641.69]

[1] CI – 95% Confidence interval, using the t-distribution.

Four load profiles are considered to match the data basis of Sections 3.2 and 3.3, recorded at low sampling rates of ~2 Hz. The overall power demand rises more gradually and peaks at a median of 15.94 s at 635 W. All profiles show the same four phases, but the phase transitions are not perfectly synchronized and show slight time variation. Figure 7 shows one of the four power profiles segmented into Starting, Ramp-up, Dome and Constant phases.

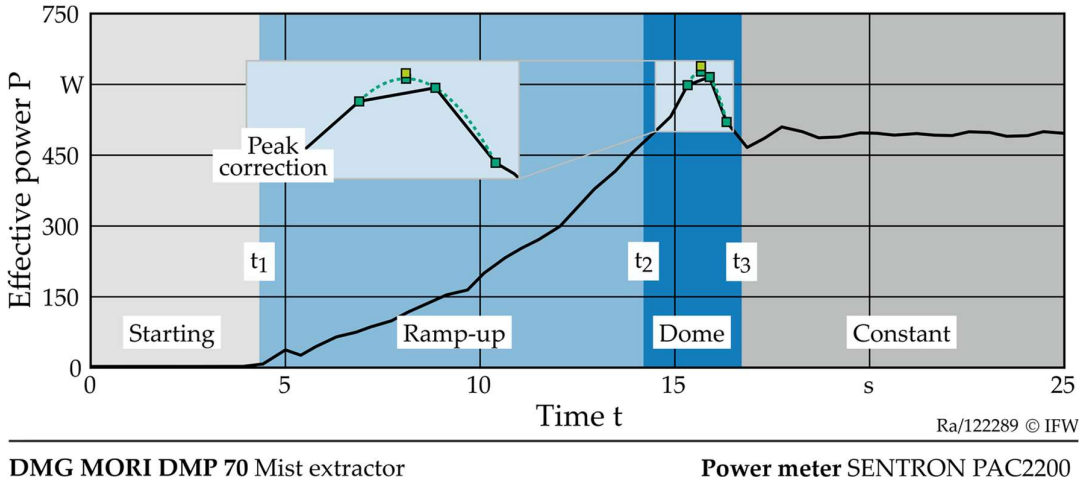

Figure 7. Power profile measurement of the DMP 70 mist extractor segmented (Starting, Ramp-up, Dome and Constant) and with peak correction.

 doi:10.20944/preprints202603.1106.v1

The segmentation was applied according to Equation 6 using the following transition points:

$$P(t) \approx \begin{cases} 0\ \mathrm{W}, & t_0 \le t < t_1, \\ P_{\mathrm{Ramp-}}(t), & t_1 \le t < t_2, \\ P_{\mathrm{Dome}}(t), & t_2 \le t < t_3, \\ P_\infty, & t \ge t_3 \end{cases} \tag{6}$$

$$t_1 := \min\{t \ge t_0 \,|\, P(t) \ge P_{\mathrm{Starting}}\}$$

$$t_2 := \min\{t \ge t_1 \,|\, P_{\mathrm{Ramp-}}(t) > P_\infty\}$$

$$t_3 := \min\{t \ge t_2 \,|\, P_{\mathrm{Dome}}(t) < P_\infty\}$$

The ramp-up begins as soon as P exceeds P_{Starting}, defined as 1% of the asymptotic power demand $P_\infty \approx 492.5$ W. When P first surpasses P_∞, the dome segment starts. The plateau segment begins when P subsequently drops below P_∞ for the first time.

For this soft starter, the threshold definitions clearly define the segments. The measured values still have to be mathematically modelled to create deployable, segment-wise functions for the two segments $P_{\mathrm{Ramp\text{-}up}}$ and P_{Dome}. As modelling approaches, those specified in the sets of Equations 7 and 8 are tested:

(**ii**) Ramp-up

$$f_{\mathrm{Quadratic}}(t; a, b, c) := at^2 + bt + c$$

$$f_{\mathrm{Logistic}}(t, y_0, A, k, t_0) := y_0 + A\frac{1}{1 + e^{-k(t-t_0)}} \tag{7}$$

$$f_{\mathrm{Exponential}}(t;\ y_0, A, k) := y_0 + Ae^{kt}$$

(**iii**) Dome

$$f_{\mathrm{DiffExp}}(t; P_\infty, K, a, b) := P_\infty + K(e^{-at} - e^{-bt})$$

$$f_{\mathrm{Parabolic}}(t;\ P_\infty, \kappa, v_0) := P_\infty - \kappa t^2 + v_0 t \tag{8}$$

$$f_{\mathrm{Alpha}}(t;\ P_\infty, C, n, a) := P_\infty + Ct^n \times e^{-at}$$

The resulting models achieve R^2-values of up to 0.94 for a quadratic fit in the ramp-up phase (a). Overall accuracy is $\Delta E = 0.92\%$. For the dome (b), a parabolic fit attains $\Delta E = 0.65\%$, though based on fewer samples. Figure 8 shows the fits for both phases.

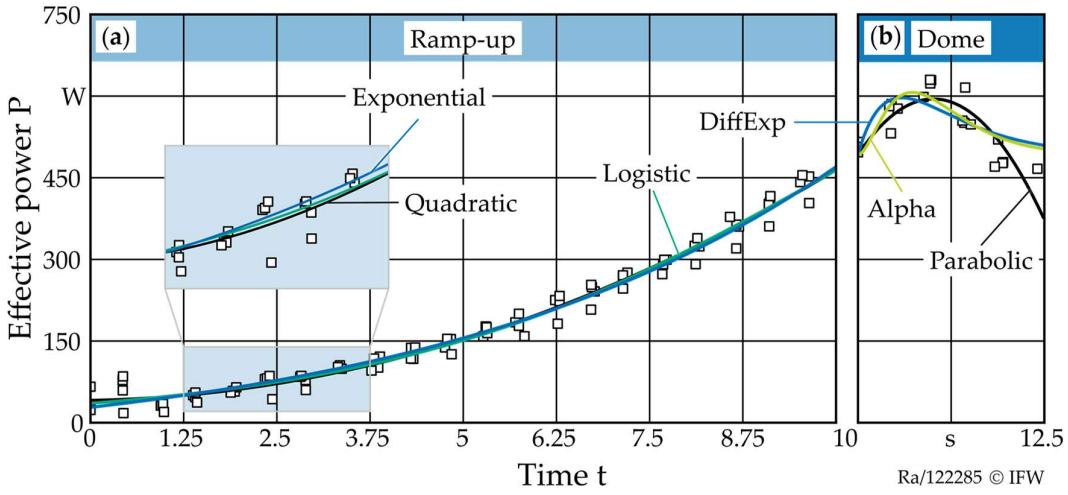

Figure 8. Ramp-up and dome fits for a soft-starting mist extractor.

 doi:10.20944/preprints202603.1106.v1

The regression parameters for the two segments are provided in Appendix A2. In conclusion, Sections 3.3 and 3.4 deliver complete, deployable power profiles for both configurations – the DOL-started mist extractor (Section 3.3) and the soft-starting mist extractor (Section 3.4).

4. Discussion and Conclusion

The premise of this study was to determine whether component models can be derived from low sampling rate data (1–2 Hz). The results show that this is possible when specific corrective measures are applied. A Nyquist-aware parabolic interpolation with curvature bias correction enabled power peak correction, improving on the standard look-up tables and heuristics commonly used.

Comparing a direct-on-line (DOL) mist extractor (Milltap 700) with a soft-started unit (DMP 70) shows the expected trade-off: the soft starter lowers the peak power demand to slightly above 0.6 kW while lengthening the transient time to ≈ 16 s. Segment-wise, parsimonious fits capture the energy demand of the auxiliary unit with small errors: $\Delta E = 0.92\%$ during ramp-up and 0.65% in the dome segment. Using these models, the power demand of a component can be estimated for any given timestamp on edge devices.

The segment-wise approach is also robust and suitable for integration into low-cost edge devices because the models rely on standard mathematical functions (e.g., logistic and exponential) that are computationally inexpensive. This improves model deployability for peak-shaving MES or related systems.

Together, these advances outline a practical path to ISO-aligned, peak-aware component modelling suitable for shop-floor deployment. In particular, the workflow enables manufacturers to create actionable component-level insights from existing power-meter data.

Author Contributions: Conceptualization, B.R. and H.B.; writing—original draft preparation, B.R.; writing—review and editing, B.R. and H.B.; supervision, B.D.

Funding: This research is conducted within the Factory-X project, which is funded by the German Federal Ministry for Economic Affairs and Energy. Factory-X contributes to the broader Manufacturing-X initiative.

Data Availability Statement: The original data presented in the study are openly available in Zenodo at https://doi.org/10.5281/zenodo.18222908.

Conflicts of Interest: The authors declare no conflicts of interest.

Abbreviations

The following abbreviations are used in this manuscript:

CA	Compressed air
CI	Confidence interval
DOL	Direct-on-line
ME	Mist extractor
MES	Manufacturing execution systems
HMI	Human machine interface
S7	Siemens S7-Protocol

Appendix A

Appendix A.1. Grid Search for the Switching Point of Modelling a DOL-Starter

In Table 5 the parameter estimates for the grid search to find the optimal combination of switching point τ and the candidate model are shown.

Table 5. Parameter estimates across switching points τ and candidate models for the grid search.

	Logistic	Exponential	DoubleExp

 doi:10.20944/preprints202603.1106.v1

τ = 5.5 s	c = 378.5075 L = 2,441.4914 k = 1.9630 t_0 = 0.2089	β_0 = 356.3591 β_1 = 1,527.6292 - T = 0.8139	β_0 = 375.5317 β_1 = 2,514.5292 β_2 = -1,043.6565 T = 0.5835
	ΔE = 0.64%	ΔE = 0.27%	ΔE = 0.62%
τ = 6 s	c = 379.2701 L = 2,432.8701 k = 1.9690 t_0 = 0.2121	β_0 = 360.4229 β_1 = 1,524.4519 - T = 0.8075	β_0 = 470.4995 β_1 = -1,023.7406 β_2 = 2,425.1845 T = 2.2640
	ΔE = 0.64%	ΔE = 0.23%	ΔE = 0.38%
τ = 6.5 s	c = 379.8889 L = 2,425.9358 k = 1.9739 t_0 = 0.2146	β_0 = 363.5319 β_1 = 1,522.0349 - T = 0.8027	β_0 = 377.6689 β_1 = 2,523.2734 β_2 = -1,054.6091 T = 0.5797
	ΔE = 0.64%	ΔE = 0.23%	ΔE = 0.62%

Appendix A.2. Model Fits and Parameters of a Soft Starter: Ramp-Up and Dome Phase

In Table 6 the parameter estimates for the three candidates in the set of Equations 7 fitted to the Ramp-up segment are shown.

Table 6. Parameters for the best fits in the Ramp-up phase.

	Parameters	RMSE	ΔE
Quadratic	a = 4.0082 b = 2.2515 c = 40.9830	16.89	0.92%
Logistic	y_0 = 1.2734 A = 967.1936 k = 0.3220 t_0 = 10.2663	17.02	0.97%
Exponential	y_0 = -58.4708 A = 86.6086 k = 0.1809	17.71	1.19%

In Table 7 the parameter estimates for the three candidates in the set of Equations 8 fitted to the Dome segment are shown.

Table 7. Parameters for the best fits in the Dome phase (using $P_\infty \approx 492.5$ W).

	Parameters	RMSE [W]	ΔE [%]
Parabolic	κ = 100.100 v_0 = 202.400	30.03	0.65%
DiffExp	κ = 8.0810×10^4 a = 1.7050 b = 1.7110	35.36	1.66%
Alpha	C = 1,589.0000 a = 2.7440 n = 2	30.29	1.83%

References

1. Denkena, B.; Abele, E.; Brecher, C.; Dittrich, M.-A.; Kara, S.; Mori, M. Energy efficient machine tools. CIRP Ann. Manuf. Technol. 2020, 69, 646–667. https://doi.org/10.1016/j.cirp.2020.05.008.
2. Mori, M.; Fujishima, M.; Inamasu, Y.; Oda, Y. A Study on Energy Efficiency Improvement for Machine Tools. *CIRP Annals—Manufacturing* Technology 2011, 60, 145–148. https://doi.org/10.1016/j.cirp.2011.03.099.

 doi:10.20944/preprints202603.1106.v1

3. Diaz, N.; Redelsheimer, E.; Dornfeld, D. Energy Consumption Characterization and Reduction Strategies for Milling Machine Tool Use. In Glocalized Solutions for Sustainability in Manufacturing; Hesselbach, J., Herrmann, C., Eds.; Springer: Berlin/Heidelberg, Germany, 2011; pp. 263–267. https://doi.org/10.1007/978-3-642-19692-8_46.
4. Denkena, B.; Helmecke, P.; Hülsemeyer, L. Energy efficient machining with optimized coolant lubrication flow rates. Procedia CIRP 2014, 24, 25–31. https://doi.org/10.1016/j.procir.2014.07.140.
5. Phoenix Contact. Technical Data—EEM-MA370. Available online: https://www.phoenixcontact.com/empro-help/rm/ref/Technical_data/EEM-MA370.htm (accessed on 9 November 2025).
6. Siemens AG. Equipment Manual—SENTRON PAC2200. Available online: https://cache.industry.siemens.com/dl/files/835/109746835/att_1123515/v2/MAN_L1V30415167B-06_en_en-US.pdf (accessed on 9 November 2025).
7. Balogun, V. A.; Mativenga, P. T. Modelling of Direct Energy Requirements in Mechanical Machining Processes. J. Clean. Prod. 2013, 41, 179–186. https://doi.org/10.1016/j.jclepro.2012.10.015.
8. Gutowski, T.; Dahmus, J.; Thiriez, A. Electrical Energy Requirements for Manufacturing Processes. In Proceedings of the 13th CIRP International Conference on Life Cycle Engineering; Leuven, Belgium, 31 May–2 June 2006; pp. 623–638. Available online: https://web.mit.edu/2.813/www/readings/Gutowski-CIRP.pdf (accessed on 26 November 2025).
9. Li, W.; Kara, S. An Empirical Model for Predicting Energy Consumption of Manufacturing Processes: A Case of Turning Process. Proc. Inst. Mech. Eng. Part B J. Eng. Manuf. 2011, 225, 1636–1646. https://doi.org/10.1177/2041297511398541.
10. Xia, T.; An, X.; Yang, H.; Jiang, Y.; Xu, Y.; Zheng, M.; Pan, E. Efficient Energy Use in Manufacturing Systems—Modeling, Assessment, and Management Strategy. Energies 2023, 16, 1095. https://doi.org/10.3390/en16031095.
11. Neugebauer, R.; Wabner, M.; Rentzsch, H.; Ihlenfeldt, S. Structure Principles of Energy Efficient Machine Tools. CIRP J. Manuf. Sci. Technol. 2011, 4, 136–147. https://doi.org/10.1016/j.cirpj.2011.06.017.
12. Denkena, B.; Mori, M.; Dittrich, M.-A.; Klages, N.; Matthies, J. Energy efficient supply of cutting fluids in machining by utilizing flow rate control. CIRP Ann. Manuf. Technol. 2023, 72, 349–352. https://doi.org/10.1016/j.cirp.2023.04.082.
13. Denkena, B.; Dittrich, M.-A.; Krüger, M.; Wertheim, R. Energy-efficient control of dust extraction for the machining of fibre-reinforced plastics. J. Clean. Prod. 2018, 182, 862–872. https://doi.org/10.1016/j.procir.2018.08.178.
14. Gontarz, A.; Roth, P.; Liebrich, T. How much energy does precision need? Minimising energy demand while maintaining accuracy. In *Proceedings of the 24th International Conference & Exhibition of the European Society for Precision Engineering and Nanotechnology (euspen 2024)*; euspen: Reggio Emilia, Italy, 2024.
15. International Organization for Standardization (ISO). *Machine tools—Environmental evaluation of machine tools—Part 1: Design methodology for energy-efficient machine tools*. ISO 14955-1:2017; International Organization for Standardization: Geneva, Switzerland, 2017. https://www.euspen.eu/knowledge-base/SUS24109.pdf
16. International Organization for Standardization (ISO). *Machine tools—Environmental evaluation of machine tools—Part 3: Principles for testing metal-cutting machine tools with respect to energy efficiency*. ISO 14955-3:2020; International Organization for Standardization: Geneva, Switzerland, 2020.
17. Klemenjak, C.; Goldsborough, P. Non-intrusive load monitoring: A review and outlook. In *Informatik* 2016; Gesellschaft für Informatik e.V.: Bonn, Germany, 2016; arXiv:1610.01191.
18. Zoha, A.; Gluhak, A.; Imran, M.A.; Rajasegarar, S. Non-intrusive load monitoring approaches for disaggregated energy sensing: A survey. *Sensors* 2012, 12, 16838–16866. https://doi.org/10.3390/s121216838.
19. Huber, P.; Calatroni, A.; Rumsch, A.; Paice, A. *Review on deep neural networks applied to low-frequency NILM. Energies* 14(9), 2390, 2021. https://doi.org/10.3390/en14092390.
20. Edem, E.; Mativenga, P. Modelling of energy demand from computer numerical control (CNC) toolpaths. J. Clean. Prod. 2017, 157, pp. 310–321. https://doi.org/10.1016/j.jclepro.2017.04.096.

 doi:10.20944/preprints202603.1106.v1

21. Jeong, S.-K.; Lee, D.-B.; Hong, K.-H. Comparison of system performance on hot-gas bypass and variable speed compressor in an oil cooler for machine tools. *J. Mech. Sci. Technol.* 2014, 28, 721–727. https://doi.org/10.1007/s12206-013-1136-1.
22. Wang, Y.; Yin, K.; Yuan, Y.; Chen, J. Current-Limiting Soft Starting Method for a High-Voltage and High-Power Motor. Energies 2019, 12, 3068. doi:10.3390/en12163068.
23. Japanese Standards Association (JSA). Machine tools—Test methods for electric power consumption—Part 1: Machining centres. JIS TS B 0024-1:2010; Japanese Standards Association: Tokyo, Japan, 2010.
24. Züst, S.; Gontarz, A.; Wegener, K. Energy equivalent of compressed air consumption in a machine tool environment. In *Innovative Solutions: Proceedings of the 11th Global Conference on Sustainable Manufacturing;* Seliger, G., Ed.; Universitätsverlag der TU Berlin: Berlin, Germany, 2013; pp. 394–399.
25. Unser, M. Sampling—50 Years After Shannon. *Proc. IEEE* **2000**, 88, 569–587. https://doi.org/10.1109/5.843002.
26. Lai, X.; Torp, H. Interpolation Methods for Time-Delay Estimation Using Cross-Correlation Method for Blood Velocity Measurement. *IEEE Trans. Ultrason. Ferroelectr. Freq. Control* **1999**, *46*, 277–290. https://doi.org/10.1109/58.753016.
27. Talvila, E.; Wiersma, M. Simple derivation of basic quadrature formulas. *Atl. Electron. J. Math.* 2012, 5, 47–59. https://doi.org/10.48550/arXiv.1202.0249.